Main Text Word Count: 4,000

Translational Evidence for Dopaminergic Rewiring of the Basal Ganglia in Persons with Schizophrenia

*Philip N. Tubiolo, MS[1,2,3], *John C. Williams, PhD[1,2,4], Roberto B. Gil, MD[2,5,6], Clifford Cassidy, PhD[2], Natalka K. Haubold, BA[2], Yash Patel, MS[2], Sameera K. Abeykoon, PhD[2], Zu Jie Zheng, BS[2,7], Dathy T. Pham[2,8], Najate Ojeil, PhD, MPH[5,6], Kelly Bobchin, BA[2], Eilon B. Silver-Frankel, BS[2], Greg Perlman, PhD[2], Jodi J. Weinstein, MD[2,5,6], Christoph Kellendonk, PhD[5,6,9], Guillermo Horga, MD, PhD[5,6], Mark Slifstein, PhD[2,5,6], Anissa Abi-Dargham, MD[1,2,5,6,10] & Jared X. Van Snellenberg, PhD[1,2,5,6,11]

*These authors contributed equally to this work

[1]Department of Biomedical Engineering, Stony Brook University, Stony Brook, NY 11794;
[2]Department of Psychiatry and Behavioral Health, Renaissance School of Medicine at Stony Brook University, Stony Brook, NY 11794;
[3]Scholars in BioMedical Sciences Training Program, Renaissance School of Medicine at Stony Brook University, Stony Brook, NY 11794;
[4]Medical Scientist Training Program, Renaissance School of Medicine at Stony Brook University, Stony Brook, NY 11794;
[5]Department of Psychiatry, Columbia University Vagelos College of Physicians and Surgeons, New York-Presbyterian / Columbia University Irving Medical Center, New York, NY 10032;
[6]New York State Psychiatric Institute, New York, NY 10032;
[7]College of Medicine, State University of New York Downstate Health Sciences University, Brooklyn, NY 11203;
[8]Department of Neurobiology and Behavior, Cornell University, Ithaca, NY 14853;
[9]Department of Molecular Pharmacology & Therapeutics, Vagelos College of Physicians and Surgeons, New York-Presbyterian / Columbia University Irving Medical Center, New York, NY 10032;
[10]Department of Radiology, Renaissance School of Medicine at Stony Brook University, Stony Brook, NY 11794;
[11]Department of Psychology, Stony Brook University, Stony Brook, NY 11794.

CORRESPONDING AUTHOR:
Jared X. Van Snellenberg
101 Nicolls Rd
Health Sciences Center 10-087J
Stony Brook, NY 11794
Tel: 631-638-0064
Jared.VanSnellenberg@stonybrookmedicine.edu

Short/Running Title: Basal Ganglia Rewiring in Schizophrenia

Keywords: Dopamine, task-based fMRI, neuromelanin-sensitive MRI, positron emission tomography, working memory, basal ganglia

Abstract

Background: In prior work, a transgenic mouse model of striatal dopamine dysfunction observed in persons with schizophrenia (PSZ) exhibited dopamine-related neuroplasticity in the basal ganglia, a phenotype has never been demonstrated in human PSZ. Consequently, we sought to identify a dopamine-related alteration of basal ganglia connectivity via working memory task-based and resting-state functional magnetic resonance imaging (fMRI), neuromelanin-sensitive MRI (NM-MRI), and positron emission tomography (PET), in unmedicated PSZ.

Methods: In this case-control study, 37 unmedicated PSZ and 30 demographically matched healthy controls (HC) underwent resting-state fMRI, with a subset of 29 PSZ and 29 HC also undergoing working memory task-based fMRI. Additionally, 22 PSZ and 20 HC underwent NM-MRI and 7 PSZ and 4 HC underwent [^{11}C]-(+)-PHNO PET with amphetamine challenge. Primary outcome measures included: 1) task-state and resting-state functional connectivity (FC) between dorsal caudate (DCa) and globus pallidus externus (GPe), 2) NM-MRI contrast-to-noise ratio in substantia nigra/ventral tegmental area voxels associated with psychotic symptom severity, and 3) baseline and amphetamine-induced change in [^{11}C]-(+)-PHNO binding potential in DCa.

Results: PSZ displayed elevated DCa-GPe task-state FC, which was associated with increased NM-MRI contrast-to-noise ratio in the substantia nigra, decreased baseline DCa D2 receptor availability, greater amphetamine-induced DCa dopamine release, and worse working memory task performance.

Conclusions: This study provides in-vivo evidence of a dopamine-associated neural abnormality of DCa and GPe connectivity in unmedicated PSZ. This phenotype suggests a potential neurodevelopmental mechanism of working memory deficits in schizophrenia, representing a critical step towards developing treatments for cognitive deficits.

Abbreviations

ANTs, Advanced Normalization Tools;

BGTC, basal ganglia-thalamo-cortical;

BOLD, blood-oxygen-level-dependent;

BP_{ND}, binding potential (non-displaceable);

CIFTI, connectivity informatics technology initiative;

CNR, contrast-to-noise ratio;

D1R, dopamine D1 receptor;

D2R, dopamine D2 receptor;

D2R-OE, dopamine D2 receptor overexpressing;

DCa, dorsal caudate;

DLPFC, dorsolateral prefrontal cortex;

DOPA, dihydroxyphenylalanine;

FC, functional connectivity;

FDR, false discovery rate;

fMRI, functional magnetic resonance imaging;

GABA, gamma-aminobutyric acid;

GEV-DV, generalized extreme value DVARS;

GPe, globus pallidus externus;

GPi, globus pallidus internus;

HC, healthy control;

HRF, hemodynamic response function;

IBZM, iodobenzamide;

IQR, interquartile range;

K_{ir}, inwardly rectifying potassium;

MNI, Montreal Neurologic Institute;

MP, motion parameter;

MSN, Medium spiny neuron;

NM-MRI, neuromelanin-sensitive magnetic resonance imaging;

NYSPI, New York State Psychiatric Institute;

PANSS, positive and negative syndrome scale;

PET, positron emission tomography;

PHNO, 4-propyl-9-hydroxynaphthoxazine;

PSZ, persons with schizophrenia;

ROI, region of interest;

RS, resting-state;

rs-FC, resting-state functional connectivity;

SD, standard deviation;

SE, standard error;

SN, substantia nigra;

SOT, self-ordered working memory task;

SPM12, Statistical Parametric Mapping 12;

STN, subthalamic nucleus;

ts-FC, task-state functional connectivity;

TE, echo time;

TR, repetition time;

VTA, ventral tegmental area;

WM, working memory

1. Introduction

Evidence of striatal dopamine dysfunction in persons with schizophrenia (PSZ) is among the most robust and consistently replicated findings in the neurobiology of schizophrenia. Studies with [^{18}F]DOPA show elevated presynaptic striatal dopamine synthesis in medication-naïve and medication-free PSZ (1, 2), as well as individuals at clinical high risk for schizophrenia (3, 4). Studies using radiolabeled dopamine D2 receptor (D2R) antagonists [^{123}I]IBZM or [^{11}C]raclopride show increased amphetamine-induced tracer displacement in striatum in PSZ (5, 6), while depletion of dopamine with alpha-methyl-para-tyrosine results in increased tracer binding in PSZ (7, 8), suggesting PSZ exhibit higher occupancy of D2 receptors due to higher synaptic levels of DA, consistent with increased presynaptic availability and release of dopamine. These findings spurred the development of a transgenic mouse model to mimic this abnormality and study the neurophysiological consequences of excess striatal D2R stimulation. D2R overexpressing (D2R-OE) mice have selectively increased expression of D2Rs in the caudate-putamen, with expression temporally controllable via doxycycline (9). D2R-OE mice display performance deficits in a delayed non-match-to-sample T-maze task that persist even if D2R overexpression is halted in adulthood (9), suggesting a neurodevelopmental cognitive deficit reminiscent of those seen in human PSZ (10, 11).

D2R-OE mice also display striking neuroplasticity within the basal ganglia-thalamo-cortical (BGTC) circuit (12), which plays critical modulatory roles in motor, limbic, and cognitive functioning (13, 14). This circuit is comprised of two functionally opposed pathways, the “direct” pathway and the “indirect” pathway (**Figure 1**). While these pathways were initially thought to be anatomically segregated, tracing studies in rats and monkeys demonstrate that some direct pathway D1R-expressing medium spiny neurons (MSNs), which project to the globus pallidus internus (GPi; entopeduncular nucleus in rodents) and substantia nigra (SN) pars reticulata, actually bifurcate and send additional collaterals to the globus pallidus externus (GPe; 15, 16); these are termed “bridging collaterals,” as they bridge the direct and indirect pathways (12).

D2R-OE mice exhibit a highly plastic increase in bridging collateral density, which decreased when the overexpression was halted by doxycycline in adult animals but returned to elevated levels when doxycycline was removed. Haloperidol, a D2 antagonist antipsychotic, also reduces bridging collateral density in D2R-OE and wildtype animals, while D2R knockdown mice exhibit dose-dependent reductions in bridging collateral density (12), demonstrating that D2R stimulation in the striatum is a causal mechanism of bridging collateral density. Functionally, this plasticity is hypothesized to be a homeostatic mechanism regulating the balance of excitability in the direct and indirect pathways: paradoxically, upregulation of D2Rs results in downregulation of inwardly-rectifying potassium (K_{ir}) channels (17), resulting in *increased* excitability of indirect pathway MSNs (in spite of D2Rs themselves being inhibitory). Thus, increased bridging collaterals from the direct pathway may counter increased indirect pathway excitability and restore the overall balance of thalamic excitation and inhibition. However, given that cognitive deficits persist in D2R-OE mice after the reversal of D2R overexpression, further neurodevelopmental abnormalities with the BGTC circuit may be present as a result of this compensatory mechanism. Notably, bridging collateral density in D2R-OE mice was greatest between associative striatum (medial caudate-putamen) and medial pallidum, which receives input from associative cortical regions such as the dorsolateral prefrontal cortex (DLPFC)(12). Similarly, higher-resolution PET imaging studies in human PSZ have shown greater baseline occupancy of D2Rs in the dorsal caudate (DCa), and more broadly in the associative striatum, as compared to ventral and sensorimotor striatum (7, 18).

Overall, these findings provide robust evidence of neuroplasticity of striatopallidal projections in response to D2R density in a transgenic mouse developed to mimic striatal dopamine dysfunction in PSZ. Here, we sought to translate these findings to human patients, hypothesizing that if this compensatory response to D2R overstimulation occurs in PSZ, it should be detectable as altered functional connectivity (FC) between the striatum (specifically DCa) and the GPe. However, available evidence also suggests that: 1) any alteration in FC may

only be observable in unmedicated PSZ, as D2R antagonists reduce the density of bridging collaterals in rodents; 2) while altered anatomical connectivity should alter DCa-GPe FC, the expected direction of change is somewhat unclear—although striatal MSNs are GABA-ergic and thus inhibitory, net inhibition of a region is still metabolically demanding and can increase functional Magnetic Resonance Imaging (fMRI) Blood Oxygen Level-Dependent (BOLD) signal (19); and finally, 3) because striatal MSNs are hyperpolarized at rest, with low baseline firing rates (20), any observed change in FC may only be apparent under conditions in which the affected basal ganglia circuitry is actively processing information and MSNs are activated. Consequently, we conducted an FC MRI study of unmedicated PSZ in both a resting state and during the performance of a working memory (WM) task that we have shown robustly activates the DCa and other striatal regions (21), in order to test whether we could observe altered DCa-GPe connectivity during rest or task that could inform our hypothesis that unmedicated PSZ have increased bridging collateral density.

Given the interconnected nature of the BGTC circuit, we also chose to implement a network modeling approach to calculating FC between regions. This addresses the “third variable” problem, in which altered FC between regions could be driven by a third region that is not accounted for in the model. For example, apparent altered striato-pallidal connectivity could be driven by altered pallido-thalamic or thalamo-cortical connectivity that then propagates through the network. Our approach calculates FC as a partial correlation controlling for timeseries in regions of interest (ROIs) outside each given ROI pair, a straightforward method that reliably distinguishes between direct and indirect network connections in simulated and *in vivo* data (22, 23).

In addition, many of our participants were also enrolled in other neuroimaging studies, which included studies of dopamine function that could further inform whether altered FC might be driven by striatal dopamine dysfunction. Thus, in two subsets of our sample, we also report on the relationship between DCa-GPe FC and dopamine function measured via 1) neuromelanin-

sensitive MRI (NM-MRI) of the SN (an indirect measure of long-term dopamine turnover that is correlated with psychotic symptoms; 24, 25) and; 2) Positron Emission Tomography (PET) with the D2/3 agonist radiotracer [^{11}C]-(+)-PHNO (26, 27) and an amphetamine challenge. Finally, we also conducted exploratory analyses examining the relationship between DCa-GPe connectivity and WM task performance and positive and negative symptoms in PSZ.

2. Methods

2.1. Overview

This is a case-control study of unmedicated PSZ and healthy controls (HC) aged 18-55 years old and demographically matched on age, parental socioeconomic status, race, and ethnicity. All procedures occurred at the New York State Psychiatric Institute (NYSPI) except PET scanning, which occurred at Yale University. PSZ were considered unmedicated if they were antipsychotic-naïve or antipsychotic-free for at least three weeks prior to recruitment. Additionally, antipsychotic-naïve participants were free from any prior use of long-acting injectable antipsychotics. All participants were free of major neurological disorders, current substance use disorders, and psychiatric disorders other than schizophrenia, schizophreniform disorder, or schizoaffective disorder. Full inclusion and exclusion criteria are described in the **Supplementary Methods.** All procedures were approved by the NYSPI and Yale Institutional Review Boards.

2.2. Participants

Thirty-seven PSZ and 30 HC completed RS fMRI, with a subset of 29 PSZ and 29 HC completing task-based fMRI. Discrepancies in participation between RS and task-based fMRI samples is due to prioritization of the RS fMRI acquisition in the study protocol; several participants terminated study participation prior to task-based fMRI acquisition. Additionally, 22 PSZ and 20 HC who performed task-based fMRI underwent NM-MRI. Finally, a smaller subset of 7 PSZ and 4 HC underwent [^{11}C]-(+)-PHNO PET with amphetamine challenge. Participants

underwent several clinical and demographic assessments described in the **Supplementary Methods**. However, given incomplete data collection in many assessments (mainly due to time constraints in participant study visits), symptomatology analyses were limited to the use of positive and negative symptom subscales from the Positive and Negative Syndrome Scale (PANSS). RS fMRI data and NM-MRI data from a subset of these participants has been previously analyzed and reported on elsewhere (24, 28), while task-based fMRI data were acquired specifically for the testing of the *a priori* hypothesis presented in this manuscript. Additionally, all PET data used here were serendipitously acquired in some of our research participants as part of an unrelated study, and are previously unpublished.

2.3. Neuroimaging Procedures

MRI equipment, sequences, and processing are described in detail in the **Supplementary Methods.** Briefly, in addition to standard structural sequences, we collected multiband fMRI scans with 2 mm isotropic voxel resolution for approximately 30 minutes each for RS and task-state FC. We employed the self-ordered working memory task(SOT; see Figure S1 for task schematic; 21, 29), and neural responses to task-events were modeled as per our prior work (21, 30). The WM task fMRI data were then residualized with respect to the modeled task-evoked activation to distinguish task-state FC (ts-FC) from task-related coactivation (31, 32). Preprocessing was conducted with the Human Connectome Project Minimal Preprocessing Pipeline (33), version 4.2.0, followed by established FC-specific processing methods from our prior work (34). Finally, ts-FC used only “task-on” volumes, which were identified as all volumes beginning two seconds after each task block onset and ending four seconds after the final trial of the block to account for the initial delay in hemodynamic response and gradual return to baseline (35).

In order to use network modeling to estimate DCa-GPe connectivity, we identified a set of regions in the BGTC circuit with established roles in cognitive and associative functions. ROIs included the mediodorsal nucleus (MD), DCa, GPe, GPi, SN, and DLPFC (see **Supplementary**

Methods for identification procedures). We omitted the subthalamic nucleus from this network model, despite its importance in the indirect pathway, due to its small size and the lack of a reliable localization technique. **Figure S2** displays the surface-based DLPFC ROI, and **Figure S3** displays the probability density of all volumetric subcortical ROIs. Note that subcortical ROI timeseries were extracted using participant-specific ROI definitions. Further, in all ROI pairs, rs-FC and ts-FC were Fisher's r-to-Z transformed and averaged across corresponding ipsilateral ROI pairs.

NM-MRI, collected in a subset of our participants, used acquisition parameters and processing procedures described elsewhere (24) and in the **Supplementary Methods**. Our NM-MRI outcome measure was the average contrast-to-noise ratio (CNR) extracted from *a priori* voxels within an overinclusive mask of the SN and ventral tegmental area (VTA) whose CNR is correlated with both psychosis severity in PSZ (measured as PANSS Positive subscale score) and subclinical positive symptom severity in persons at clinical high risk for developing a psychotic disorder (24, 25).

PET data were acquired using procedures described elsewhere (36) and in the **Supplementary Methods**. Final outcome measures included both baseline binding potential (BP_{ND}) and the fractional change in BP_{ND} following amphetamine administration,

$\frac{\mathrm{BP_{ND}(post-amph.)}}{\mathrm{BP_{ND}(baseline)}} - 1$ (ΔBP_{ND}), within a hand-drawn DCa ROI.

2.4. Statistical Analysis

Effect sizes for group differences in continuous variables were calculated using Hedges' *g* or Cliff's delta *d* for normally distributed and non-normal samples, respectively; data normality was determined via Lilliefors test with a null hypothesis that data originates from a normal distribution at significance level $p<0.05$. P-values for group differences in continuous demographic variables and clinical assessments were obtained via independent samples t-tests or Mann-Whitney U-

tests, dependent on data normality. Effect sizes for categorical and dichotomous variables were calculated as Cramér's *V* and phi coefficients, respectively, with p-values calculated using Chi-squared tests with significance level $p<0.05$. Group differences in SOT performance (29) and the proportion of correct responses in the SOT, both between HC and PSZ and between medication-naïve and medication-free PSZ, were assessed using Mann-Whitney U-tests.

Group differences in ROI pair FC were assessed via independent samples t-tests or Mann-Whitney U-tests, dependent on data normality. The primary hypothesis investigating group differences in DCa-GPe rs-FC and ts-FC was assessed for significance at $\alpha=0.05$ with Dunn–Šidák correction for two comparisons. Post-hoc tests of group connectivity differences between all other ROI pairs were assessed at $\alpha=0.05$ with false discovery rate (FDR) correction across all tests (37). Additionally, we assessed differences in DCa-GPe rs-FC and ts-FC in medication-naïve versus medication-free PSZ. As a supplementary analysis, we also assessed for group differences in DCa-GPe ts-FC and rs-FC using a robust multivariable linear regression with a Huber weight function with age and sex at birth as covariates.

Associations between DCa-GPe ts-FC and either SOT performance (measured as WM capacity k; 29), average SN/VTA NM-MRI signal, [^{11}C]-(+)-PHNO baseline BP_{ND}, or ΔBP_{ND} were assessed via robust multivariable linear regression with a Huber weight function with age, sex at birth, and diagnosis as covariates; associations with PANSS positive and negative symptoms scores were assessed in PSZ only, using the same covariates above except diagnosis. FDR correction at $\alpha=0.05$ was applied over the tests for associations with SN-VTA NM-MRI signal, baseline BP_{ND}, and ΔBP_{ND} as they constitute a family of tests concerning dopamine tone and function. All betas are reported as standardized regression coefficients β^*.

In a final set of supplementary analyses, group differences in DCa-GPe ts-FC and rs-FC, as well as associations between FC and NM-MRI signal, [^{11}C]-(+)-PHNO PET metrics, and SOT performance were repeated with smoking status included as a covariate; nicotine is a known modulator of midbrain dopamine function (38).

3. Results

3.1. Demographics

Thirty-seven PSZ and 30 HC completed at least two runs of resting-state fMRI (N=67), with zero participants excluded for excess motion. Additionally, 29 PSZ and 29 HC completed at least two runs of task-based fMRI (N=58), after excluding four participants due to excess motion. A summary table of demographic information for each cohort is shown in **Table 1**.

Group differences in SOT working memory capacity (*k*) and the proportion of correct responses are shown in **Figure S4**. The median [IQR] SOT *k* for HC and PSZ were 5.92 [1.61] and 4.73 [3.42], respectively (*P*=0.127). The median [IQR] proportion of correct responses in HC and PSZ were 0.94 [0.08] and 0.88 [0.23], respectively (*P*=0.139). Notably, in comparison to medication-free PSZ, medication-naïve PSZ displayed greater task performance (median [IQR] proportion correct of 0.83 [0.21] in medication-free and 0.97 [0.15] in medication-naïve, *P*=0.018) and SOT *k* (median [IQR] of 3.64 [4.60] in medication-free and 5.94 [2.90] in medication-naïve, *P*=0.031).

3.2. Resting-state and Task-state Functional Connectivity

Between DCa and GPe (ROIs shown in **Figure 2A, B**), no significant group difference in resting-state functional connectivity (rs-FC) was observed via Mann-Whitney U-test (median [IQR] of 0.05 [0.16] in HC and 0.08 [0.12] in PSZ, *P*=0.233; **Figure 2C**) or via robust regression while covarying for age and sex at birth (N = 67; β* [SE] = 0.12 [0.10], *P*=0.25; **Table S1**). PSZ displayed elevated ts-FC between DCa and GPe relative to HC that survives Dunn–Šidák correction (mean [SD] of 0.05 [0.09] in HC and 0.11 [0.10] in PSZ, *P*=0.0252**; Figure 2D**). This group difference in ts-FC remained statistically significant when controlling for age and sex at birth via robust regression (N = 58; β* [SE] = 0.27 [0.14], *P*=0.048**; Table S2**). The group difference in DCa-GPe ts-FC remained significant when additionally controlling for smoking

status (N = 57; β* [SE] = 0.36 [0.13], *P*=0.008**; Table S3**), while no group difference in rs-FC was observed (N = 65; β* [SE] = 0.09 [0.11], *P*=0.386**; Table S4**).

No significant differences between medication-naïve and medication-free PSZ were observed in DCa-GPe ts-FC (mean [SD] of 0.12 [0.11] in medication-free and 0.10 [0.09] in medication-naïve, *P*=0.638) or rs-FC (median [IQR] of 0.07 [0.10] in medication-free and 0.08 [0.15] in medication-naïve, *P*=0.891).

Within other direct connections in the BGTC circuit, HC displayed greater MD-DCa rs-FC than PSZ (mean [SD] of 0.27 [0.12] in HC and 0.17 [0.15] in PSZ, *P*=0.005**; Figure S5H**). No significant differences in ts-FC were observed following FDR correction (**Figure S6**), although MD-DLPFC ts-FC was elevated in PSZ before correction.

3.3. Neuromelanin-Sensitive MRI

The average NM-MRI contrast-ratio map across participants is shown in **Figure 3A**. In the *a priori* psychosis-associated voxels (24, 25), average SN/VTA NM-MRI contrast was positively associated with DCa-GPe ts-FC (N = 42; β* [SE] = 0.40 [0.17], *P*=0.023**; Figure 3B**, **Table S5**) when controlling for age, sex at birth, and diagnosis, and survives FDR correction at α=0.05. This association remains significant when controlling for smoking status (N = 42; β* [SE] = 0.41 [0.18], *P*=0.031**; Table S6**).

3.4. [^{11}C]-(+)-PHNO Positron Emission Tomography

In the subset of seven PSZ and four HC that completed both WM task-based fMRI and [^{11}C]-(+)-PHNO PET, elevated DCa-GPe ts-FC was found to be significantly negatively associated with DCa baseline D2R availability, measured as [^{11}C]-(+)-PHNO BP_{ND} (N = 11; β* [SE] = -0.45 [0.17], *P*=0.039; **Figure 3C, Table S7**). Additionally, greater DCa-GPe ts-FC was associated with more negative DCa ΔBP_{ND} (N = 11; β* [SE] = -0.82 [0.27], *P*=0.021; **Figure 3D**, **Table S7**), where a more negative ΔBP_{ND} indicates greater fractional decrease in BP_{ND} following amphetamine administration. Both results survive FDR correction at α=0.05. After controlling for

smoking status, there are no significant associations between DCa-GPe ts-FC and baseline BP_{ND} (N = 11; β* [SE] = -0.29 [0.38], *P*=0.476, **Table S8**) or ΔBP_{ND} (N = 11; β* [SE] = -0.49 [0.52], *P*=0.392, **Table S8**).

3.5. Associations between Task-state Functional Connectivity and Symptomatology

Elevated DCa-GPe ts-FC was associated with lower SOT *k* across all participants (N = 58; β* [SE] = -0.31 [0.13], *P*=0.020**; Figure 4A**, **Table S9**). This association remains significant when controlling for smoking status (N = 57; β* [SE] = -0.37 [0.13], *P*=0.008; **Table S10**). In PSZ, no significant associations were observed between DCa-GPe ts-FC and PANSS positive symptom score (N = 27; β* [SE] = -0.39 [0.21], *P*=0.068**; Figure 4B, Table S5**) or PANSS Negative symptom score (N = 27; β* [SE] = -0.20 [0.23], *P*=0.389**; Figure 4C, Table S5**).

4. Discussion

The results presented here support our hypothesis of specifically altered dorsal caudate-globus pallidus externus (DCa-GPe) connectivity in unmedicated persons with schizophrenia, which we developed *a priori* based on evidence of neuroanatomical reorganization of this circuitry in the dopamine D2 receptor overexpressing (D2R-OE) mouse model (9, 12) of striatal dopamine dysfunction in schizophrenia. Notably, our findings also provide multiple lines of evidence that this alteration is associated with striatal dopamine dysfunction, in addition to working memory (WM) deficits, consistent with the dopamine dysfunction and WM deficits in the D2R-OE mice that spurred this investigation. While DCa-GPe rs-FC findings were negative, we demonstrated DCa-GPe hyperconnectivity in unmedicated PSZ during the performance of a WM task, a condition we tested specifically because striatal MSNs that project to GPe are relatively quiet at resting state due to a negative intrinsic resting membrane potential. This may prevent the detection of altered fMRI connectivity unless receiving stimulation from cortical and thalamic inputs during cognitive processing. Critically, the full set of secondary analyses are also entirely consistent with our hypotheses, with significant correlations between DCa-GPe ts-FC

and WM as well as all dopaminergic outcome measures collected in our sample, and with DCa-GPe ts-FC being specifically elevated, rather than part of a broader alteration of ts-FC throughout the BGTC network (see **Figure S6**). While our findings cannot directly establish that elevated DCa-GPe ts-FC in PSZ is a result of upregulated bridging collaterals from D1R-containing MSNs to the GPe, we developed a direct, falsifiable, experimental test of the hypothesis that unmedicated PSZ exhibit a similar upregulation of bridging collaterals as has been observed in D2R-OE mice, and found formal support for this conclusion.

Our findings suggest a pivotal role of subcortical dopamine dysfunction in striato-pallidal neuronal reorganization. NM-MRI signal in the SN and VTA is a proxy measure of long-term dopamine turnover (unless neuronal cell death has occurred, e.g. in Parkinson's disease; 24, 25) that has been shown to be associated with the severity of psychotic symptoms (39). Elevated nigral NM signal suggests upregulated dopamine turnover in nigral cell bodies, which likely results in elevated presynaptic availability and release in striatum (40), a well-established finding in PSZ linked to psychosis severity (5, 7, 8, 18). Although observed in a small, exploratory sample of PSZ and HC, our finding that individuals who show stronger dopamine release following amphetamine challenge have more greatly elevated DCa-GPe connectivity directly supports this interpretation. Similarly, decreased baseline D2R availability was also associated with DCa-GPe hyperconnectivity, consistent with increased baseline availability of dopamine in the DCa that competes with radiotracer binding, resulting in lower BP_{ND} in these participants. However, we cannot rule out the possibility that lower D2R density in DCa also contributes to lower BP_{ND}.

Finally, we found that elevated DCa-GPe ts-FC is associated with poorer WM task performance, analogous to the performance deficits in a delayed non-match to sample T-maze in D2R-OE mice. Given that these deficits in D2R-OE mice remained when upregulation of DCa-GPe bridging collaterals was normalized via D2R antagonist antipsychotic administration, this finding suggests that DCa-GPe hyperconnectivity may be a state-dependent predictor of the

neurodevelopmental impact of persistent dopamine dysfunction in PSZ prior to becoming medicated. That is, unmedicated PSZ with more severe subcortical dopamine dysfunction develop greater bridging collateral density between DCa and GPe, thus driving further BGTC circuit reorganization that directly disrupts the maintenance of internal representations of task stimuli in prefrontal cortical regions; e.g., via effects on D1R function in DLPFC, which is thought to be disrupted in SCZ (41), critical for WM, and altered in D2R-OE mice (9, 17). A potential mechanism for this resulting cortical dysfunction is the persistent functional abnormalities that have been shown to exist in dopamine neurons of D2R-OE mice, particularly decreased phasic activity and neuronal recruitment under WM task demands (42). These abnormalities may not be normalized via antipsychotic medication given after their development, resulting in the persistence of WM deficits.

While the results presented here are consistent with the hypothesis of dopamine-driven alterations to DCa-GPe connectivity in PSZ, several caveats and limitations must be acknowledged. First, alternative interpretations of elevated DCa-GPe ts-FC in PSZ may be plausible given that rs-fMRI and task-based fMRI do not carry information on structural abnormalities. Therefore, follow-up work should utilize diffusion tensor imaging to investigate alterations in DCa-GPe structural connectivity. Next, limitations in sample size in both the RS fMRI and PET samples may limit the generalizability of the presented results. While larger than the task-based fMRI sample, the RS fMRI sample may have lacked statistical power to detect significant group differences in DCa-GPe connectivity at smaller effect sizes, although the observed difference trended in the expected direction. However, the RS fMRI sample did possess sufficient power to detect a larger effect in MD-DCa hypoconnectivity in PSZ, a finding consistent with previous work (43-45). The PET sample should be considered preliminary, as it was a small sample of PSZ and HC with markedly younger PSZ than other samples in this study. Further, associations between PET metrics and DCa-GPe tb-FC did not survive when using smoking status as a covariate. Thus, we cannot claim that associations between DCa

baseline and ΔBP_{ND} and DCa-GPe ts-FC will generalize to larger samples of PSZ with more age and substance use variation. Finally, no significant associations were observed between DCa-GPe ts-FC and PANSS Positive score. While we may have expected DCa-GPe connectivity to be an overall marker of disease severity, the lack of significant association may arise from statistical power concerns. Alternatively, DCa-GPe connectivity may more closely index the severity of a phenotype that leads to WM deficits in PSZ, rather than psychotic symptoms. This proposition would ideally be studied in a larger, transdiagnostic samples of WM task-based fMRI.

In summary, this study provides in-vivo translational evidence of a neural abnormality between the DCa and GPe in unmedicated PSZ, emulating findings from the D2R-OE transgenic mouse model. This abnormality was observed in the form of elevated FC during WM task engagement and was associated with poor WM task performance and disrupted subcortical dopaminergic function measured by two imaging modalities. Future work should aim to demonstrate structural evidence of altered DCa-GPe anatomical connectivity, as well as examine the role of D2R antagonist antipsychotic medication in the normalization of the phenotype. Nevertheless, these results build on a rich literature implicating subcortical dopaminergic dysfunction in the pathophysiology of SCZ to suggest a neurodevelopmental mechanism of WM deficits in PSZ, a crucial step towards the development of novel therapeutic targets and treatments.

5. Data and Code Availability

All data and analysis code used in the preparation of this manuscript can be made available upon request to the corresponding author through a formal data sharing agreement.

6. Acknowledgements

Research reported in this publication was supported by the National Institute of Mental Health of the National Institutes of Health (NIH) under award numbers K01MH107763 to

J.X.V.S., K23MH101637 to G.H., R01MH109635 to A.A-D., R01MH124858 to C.K., F30MH122136 to J.C.W, and K23MH115291 to J.J.W. P.N.T. was supported by the Stony Brook University Scholars in Biomedical Sciences Program (NIH Award No. T32GM148331; PI: Dr. Styliani-Anna [Stella] E. Tsirka). J.C.W. was also supported by a Research Supplement to Promote Diversity in Health-Related Research (3R01MH120293-04S1) and by the Stony Brook University Medical Scientist Training Program (Award Nos. T32GM008444 and T32GM158461; Principal Investigator: Dr. Michael A. Frohman). The Stony Brook high-performance SeaWulf computing system was supported by National Science Foundation (NSF) Award Nos. 1531492 (PI: Dr. Robert Harrison; co-PI: Dr. Yuefan Deng) and 2215987 (PI: Dr. Robert Harrison; co-PIs: Dr. Yuefan Deng, Dr. Eva Siegmann, and David Cyrille), and matching funds from the Empire State Development's Division of Science, Technology and Innovation (NYSTAR) program contract C210148. The Stony Brook University Social, Cognitive, and Affective Neuroscience (SCAN) Center was supported by NSF Award No. 0722874 (PI: Dr. Turhan Canli). This content is solely the responsibility of the authors and does not necessarily represent the official views of the NIH, NSF, or NYSTAR.

The authors would like to thank Jaeyop Jeong, Sam R. Luceno, and Srineil Nizamabad for their contributions to fMRI preprocessing, Elizabeth Chan for assistance with data visualization, and Tram N.B. Nguyen and Dr. Benjamin A. Ely for helpful discussions. We would also like to acknowledge the substantial computing resources and technical assistance provided by Stony Brook Medicine Research Computing, with substantial support from Allen Zawada and James Xikis, as well as Stony Brook Research Computing and Cyberinfrastructure and the Institute for Advanced Computational Science at Stony Brook University for access to the high-performance SeaWulf computing system, with notable support from Fırat Coşkun, Daniel Wood, and David Carlson.

7. Disclosures

Drs. Cassidy and Horga are inventors on patents for the analysis of NM-MRI, licensed to Terran Biosciences, Inc., but have received no royalties. Drs. Cassidy and Horga have an investigator-initiated sponsored research agreement and a licensing agreement with Terran Biosciences, Inc. Dr. Slifstein reports having served as a paid consultant for Neurocrine Biosciences, Inc. and for Yale University. Dr. Abi-Dargham received consulting fees from Neurocrine Biosciences, Inc., from Abbvie, Inc., and from MapLight Therapeutics, Inc. Dr. Abi-Dargham holds stock options in Herophilus, Inc. and in Terran Biosciences, Inc. Dr. Abi-Dargham is a Deputy Editor for the journal *Biological Psychiatry*. All other authors report no competing interests.

References

1. Meyer-Lindenberg A, Miletich RS, Kohn PD, Esposito G, Carson RE, Quarantelli M, et al. (2002): Reduced prefrontal activity predicts exaggerated striatal dopaminergic function in schizophrenia. *Nature Neuroscience*. 5:267-271.

2. McGowan S, Lawrence AD, Sales T, Quested D, Grasby P (2004): Presynaptic Dopaminergic Dysfunction in Schizophrenia. *Archives of General Psychiatry*. 61.

3. Egerton A, Chaddock CA, Winton-Brown TT, Bloomfield MAP, Bhattacharyya S, Allen P, et al. (2013): Presynaptic Striatal Dopamine Dysfunction in People at Ultra-high Risk for Psychosis: Findings in a Second Cohort. *Biological Psychiatry*. 74:106-112.

4. Howes OD, Bose SK, Turkheimer F, Valli I, Egerton A, Valmaggia LR, et al. (2011): Dopamine Synthesis Capacity Before Onset of Psychosis: A Prospective [18F]-DOPA PET Imaging Study. *American Journal of Psychiatry*. 168:1311-1317.

5. Abi-Dargham A, Gil R, Krystal J, Baldwin RM, Seibyl JP, Bowers M, et al. (1998): Increased striatal dopamine transmission in schizophrenia: confirmation in a second cohort. *Am J Psychiatry*. 155:761-767.

6. Breier A, Su TP, Saunders R, Carson RE, Kolachana BS, de Bartolomeis A, et al. (1997): Schizophrenia is associated with elevated amphetamine-induced synaptic dopamine concentrations: Evidence from a novel positron emission tomography method. *Proceedings of the National Academy of Sciences*. 94:2569-2574.

7. Kegeles LS, Abi-Dargham A, Frankle WG, Gil R, Cooper TB, Slifstein M, et al. (2010): Increased Synaptic Dopamine Function in Associative Regions of the Striatum in Schizophrenia. *Archives of General Psychiatry*. 67.

8. Abi-Dargham A, Rodenhiser J, Printz D, Zea-Ponce Y, Gil R, Kegeles LS, et al. (2000): Increased baseline occupancy of D2 receptors by dopamine in schizophrenia. *Proc Natl Acad Sci U S A*. 97:8104-8109.

9. Kellendonk C, Simpson EH, Polan HJ, Malleret G, Vronskaya S, Winiger V, et al. (2006): Transient and Selective Overexpression of Dopamine D2 Receptors in the Striatum Causes Persistent Abnormalities in Prefrontal Cortex Functioning. *Neuron*. 49:603-615.

10. Lee J, Park S (2005): Working Memory Impairments in Schizophrenia: A Meta-Analysis. *Journal of Abnormal Psychology*. 114:599-611.

11. Park S (1992): Schizophrenics Show Spatial Working Memory Deficits. *Archives of General Psychiatry*. 49.

12. Cazorla M, de Carvalho FD, Chohan MO, Shegda M, Chuhma N, Rayport S, et al. (2014): Dopamine D2 receptors regulate the anatomical and functional balance of basal ganglia circuitry. *Neuron*. 81:153-164.

13. Alexander GE, Crutcher MD, DeLong MR (1991): Chapter 6 Basal ganglia-thalamocortical circuits: Parallel substrates for motor, oculomotor, “prefrontal” and “limbic” functions. *The Prefrontal Its Structure, Function and Cortex Pathology*, pp 119-146.

14. Leisman G, Braun-Benjamin O, Melillo R (2014): Cognitive-motor interactions of the basal ganglia in development. *Front Syst Neurosci*. 8:16.

15. Lévesque M, Parent A (2005): The striatofugal fiber system in primates: A reevaluation of its organization based on single-axon tracing studies. *Proceedings of the National Academy of Sciences*. 102:11888-11893.

16. Labouesse MA, Torres-Herraez A, Chohan MO, Villarin JM, Greenwald J, Sun X, et al. (2023): A non-canonical striatopallidal Go pathway that supports motor control. *Nature Communications*. 14.

17. Cazorla M, Shegda M, Ramesh B, Harrison NL, Kellendonk C (2012): Striatal D2 Receptors Regulate Dendritic Morphology of Medium Spiny Neurons via Kir2 Channels. *The Journal of Neuroscience*. 32:2398-2409.

18. Howes OD, Kambeitz J, Kim E, Stahl D, Slifstein M, Abi-Dargham A, et al. (2012): The Nature of Dopamine Dysfunction in Schizophrenia and What This Means for Treatment. *Archives of General Psychiatry*. 69.

19. Jueptner M, Weiller C (1995): Review: Does Measurement of Regional Cerebral Blood Flow Reflect Synaptic Activity?—Implications for PET and fMRI. *NeuroImage*. 2:148-156.

20. Kreitzer AC (2009): Physiology and Pharmacology of Striatal Neurons. *Annual Review of Neuroscience*. 32:127-147.

21. Van Snellenberg JX, Slifstein M, Read C, Weber J, Thompson JL, Wager TD, et al. (2015): Dynamic shifts in brain network activation during supracapacity working memory task performance. *Human Brain Mapping*. 36:1245-1264.

22. Smith SM, Miller KL, Salimi-Khorshidi G, Webster M, Beckmann CF, Nichols TE, et al. (2011): Network modelling methods for FMRI. *NeuroImage*. 54:875-891.

23. Marrelec G, Krainik A, Duffau H, Pélégrini-Issac M, Lehéricy S, Doyon J, et al. (2006): Partial correlation for functional brain interactivity investigation in functional MRI. *NeuroImage*. 32:228-237.

24. Cassidy CM, Zucca FA, Girgis RR, Baker SC, Weinstein JJ, Sharp ME, et al. (2019): Neuromelanin-sensitive MRI as a noninvasive proxy measure of dopamine function in the human brain. *Proceedings of the National Academy of Sciences*. 116:5108-5117.

25. Wengler K, Baker SC, Velikovskaya A, Fogelson A, Girgis RR, Reyes-Madrigal F, et al. (2024): Generalizability and Out-of-Sample Predictive Ability of Associations Between Neuromelanin-Sensitive Magnetic Resonance Imaging and Psychosis in Antipsychotic-Free Individuals. *JAMA Psychiatry*. 81.

26. Rabiner EA, Laruelle M (2010): Imaging the D3 receptor in humans in vivo using [11C](+)-PHNO positron emission tomography (PET). *The International Journal of Neuropsychopharmacology*. 13.

27. Caravaggio F, Nakajima S, Borlido C, Remington G, Gerretsen P, Wilson A, et al. (2014): Estimating Endogenous Dopamine Levels at D2 and D3 Receptors in Humans using the Agonist Radiotracer [11C]-(+)-PHNO. *Neuropsychopharmacology*. 39:2769-2776.

28. Williams JC, Tubiolo PN, Gil RB, Zheng ZJ, Silver-Frankel EB, Haubold NK, et al. (2025): Auditory and Visual Thalamocortical Connectivity Alterations in Unmedicated People With Schizophrenia: An Individualized Sensory Thalamic Localization and Resting-State Functional Connectivity Study. *Biological Psychiatry: Cognitive Neuroscience and Neuroimaging*.

29. Van Snellenberg JX, Conway ARA, Spicer J, Read C, Smith EE (2014): Capacity estimates in working memory: Reliability and interrelationships among tasks. *Cognitive, Affective, & Behavioral Neuroscience*. 14:106-116.

30. Van Snellenberg JX, Girgis RR, Horga G, van de Giessen E, Slifstein M, Ojeil N, et al. (2016): Mechanisms of Working Memory Impairment in Schizophrenia. *Biological Psychiatry*. 80:617-626.

31. Gratton C, Laumann TO, Nielsen AN, Greene DJ, Gordon EM, Gilmore AW, et al. (2018): Functional Brain Networks Are Dominated by Stable Group and Individual Factors, Not Cognitive or Daily Variation. *Neuron*. 98:439-452.e435.

32. Elliott ML, Knodt AR, Cooke M, Kim MJ, Melzer TR, Keenan R, et al. (2019): General functional connectivity: Shared features of resting-state and task fMRI drive reliable and heritable individual differences in functional brain networks. *Neuroimage*. 189:516-532.

33. Glasser MF, Sotiropoulos SN, Wilson JA, Coalson TS, Fischl B, Andersson JL, et al. (2013): The minimal preprocessing pipelines for the Human Connectome Project. *NeuroImage*. 80:105-124.

34. Williams JC, Tubiolo PN, Luceno JR, Van Snellenberg JX (2022): Advancing motion denoising of multiband resting-state functional connectivity fMRI data. *NeuroImage*. 249.

35. Fair DA, Schlaggar BL, Cohen AL, Miezin FM, Dosenbach NUF, Wenger KK, et al. (2007): A method for using blocked and event-related fMRI data to study “resting state” functional connectivity. *NeuroImage*. 35:396-405.

36. van de Giessen E, Weinstein JJ, Cassidy CM, Haney M, Dong Z, Ghazzaoui R, et al. (2017): Deficits in striatal dopamine release in cannabis dependence. *Mol Psychiatry*. 22:68-75.

37. Benjamini Y, Hochberg Y (2018): Controlling the False Discovery Rate: A Practical and Powerful Approach to Multiple Testing. *Journal of the Royal Statistical Society: Series B (Methodological)*. 57:289-300.

38. Pidoplichko VI, DeBiasi M, Williams JT, Dani JA (1997): Nicotine activates and desensitizes midbrain dopamine neurons. *Nature*. 390:401-404.

39. van der Pluijm M, Wengler K, Reijers PN, Cassidy CM, Tjong Tjin Joe K, de Peuter OR, et al. (2024): Neuromelanin-Sensitive MRI as Candidate Marker for Treatment Resistance in First-Episode Schizophrenia. *American Journal of Psychiatry*. 181:512-519.

40. Vano LJ, McCutcheon RA, Rutigliano G, Kaar SJ, Finelli V, Nordio G, et al. (2024): Mesostriatal Dopaminergic Circuit Dysfunction in Schizophrenia: A Multimodal Neuromelanin-Sensitive Magnetic Resonance Imaging and [18F]-DOPA Positron Emission Tomography Study. *Biological Psychiatry*. 96:674-683.

41. Abi-Dargham A, Javitch JA, Slifstein M, Anticevic A, Calkins ME, Cho YT, et al. (2022): Dopamine D1R Receptor Stimulation as a Mechanistic Pro-cognitive Target for Schizophrenia. *Schizophrenia Bulletin*. 48:199-210.

42. Duvarci S, Simpson EH, Schneider G, Kandel ER, Roeper J, Sigurdsson T (2018): Impaired recruitment of dopamine neurons during working memory in mice with striatal D2 receptor overexpression. *Nature Communications*. 9.

43. Anticevic A, Yang G, Savic A, Murray JD, Cole MW, Repovs G, et al. (2014): Mediodorsal and Visual Thalamic Connectivity Differ in Schizophrenia and Bipolar Disorder With and Without Psychosis History. *Schizophrenia Bulletin*. 40:1227-1243.

44. Welsh RC, Chen AC, Taylor SF (2008): Low-Frequency BOLD Fluctuations Demonstrate Altered Thalamocortical Connectivity in Schizophrenia. *Schizophrenia Bulletin*. 36:713-722.

45. Smith Y, Raju D, Nanda B, Pare J-F, Galvan A, Wichmann T (2009): The thalamostriatal systems: Anatomical and functional organization in normal and parkinsonian states. *Brain Research Bulletin*. 78:60-68.

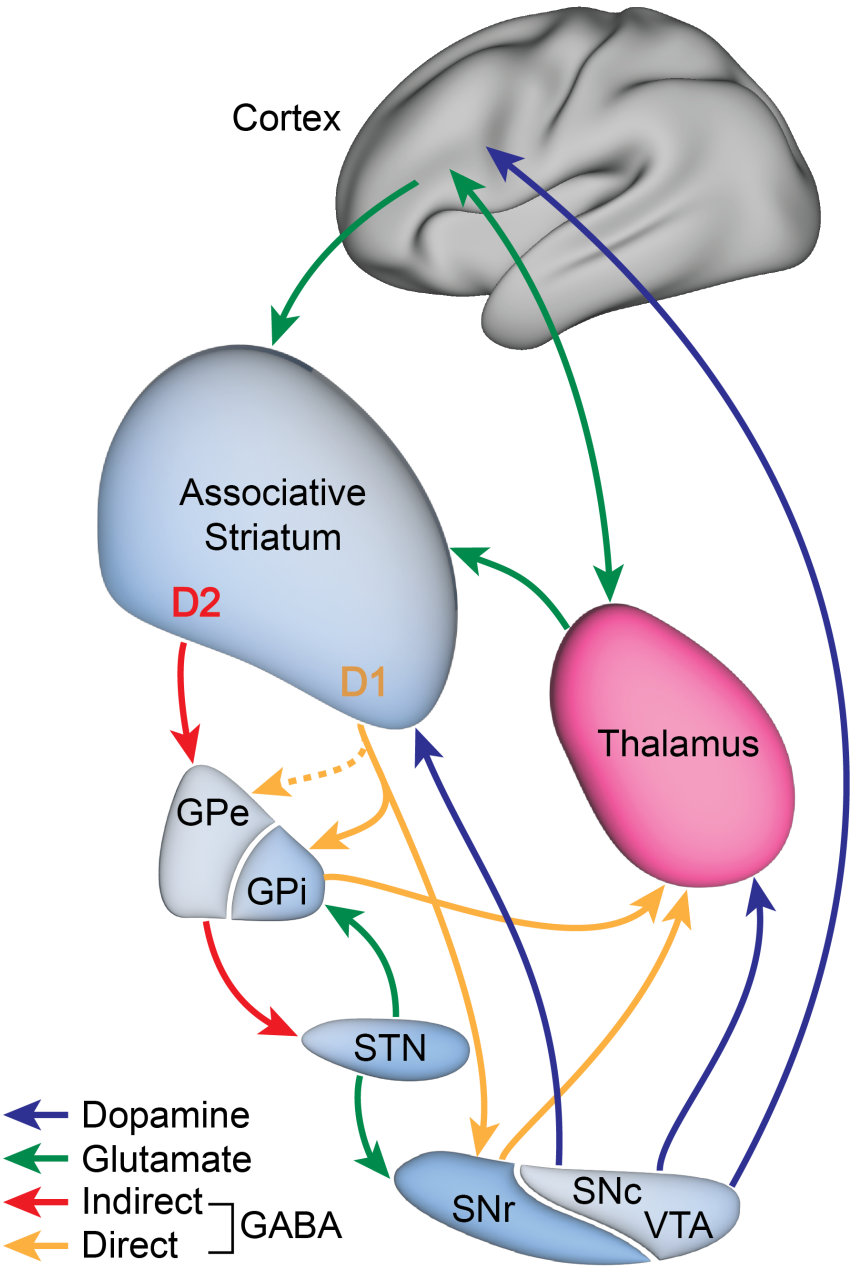

Figure 1. Schematic of basal ganglia-thalamo-cortical circuitry, highlighting glutamatergic (green arrows), GABAergic (red and orange arrows), and dopaminergic (blue arrows) connections between regions. Orange dashed line represents bridging collateral axonal projections from the associative striatum (primarily dorsal caudate) to the globus pallidus externus (GPe). GPi = globus pallidus internus; STN = subthalamic nucleus; SNr = substantia nigra pars reticulata; SNc = substantia nigra pars compacta; VTA = ventral tegmental area.

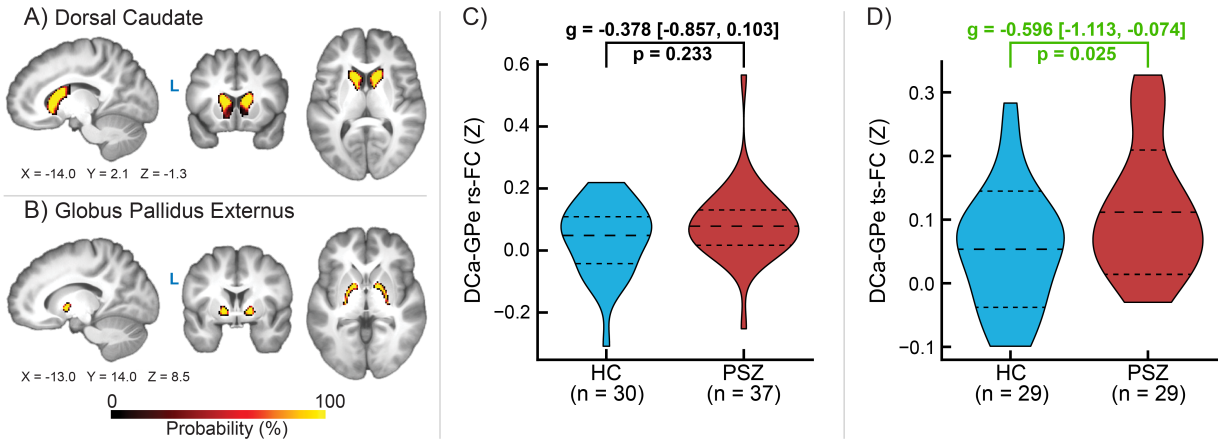

Figure 2. Probability density of A) dorsal caudate (DCa) and B) globus pallidus externus (GPe) regions of interest in the task-based fMRI sample (N = 58), as well as group differences in DCa-GPe resting-state functional connectivity (rs-FC; panel C) and task-state functional connectivity (ts-FC; panel D) between healthy controls (HC) and persons with schizophrenia (PSZ). Long-dashed and short-dashed lines denote median and interquartile range in panel C (due to non-normal data) and means and standard deviations in panel D. FC was calculated controlling for the average timeseries in dorsolateral prefrontal cortex, globus pallidus internus, substantia nigra, and mediodorsal nucleus. *g* = Hedges' *g* [95% Confidence Intervals]

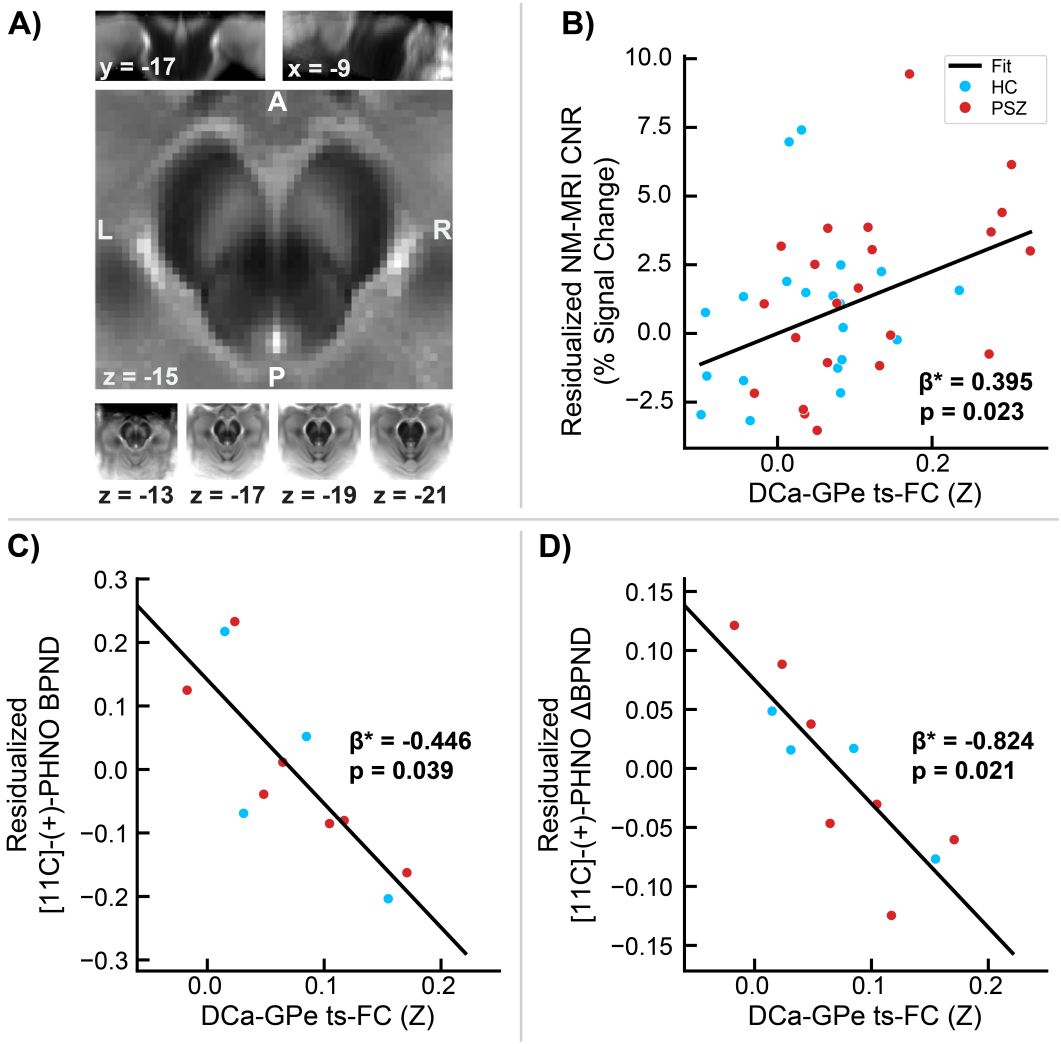

Figure 3. A) Average neuromelanin-sensitive MRI (NM-MRI) contrast-to-noise ratio (CNR) image across all participants (N = 42). B) Association between average substantia nigra – ventral tegmental area NM-MRI CNR and task-state functional connectivity (ts-FC) between dorsal caudate (DCa) and globus pallidus externus (GPe), controlling for age, sex at birth, and diagnosis (N = 42); blue dots denote healthy controls, while red dots denote people with schizophrenia. Associations between C) [^{11}C]-(+)-PHNO Baseline BPND (N = 11) or D) ΔBPND (N = 11) following amphetamine challenge and DCa-GPe ts-FC controlling for age, sex at birth, and diagnosis. Regression plot inlay shows standardized regression coefficient β*.

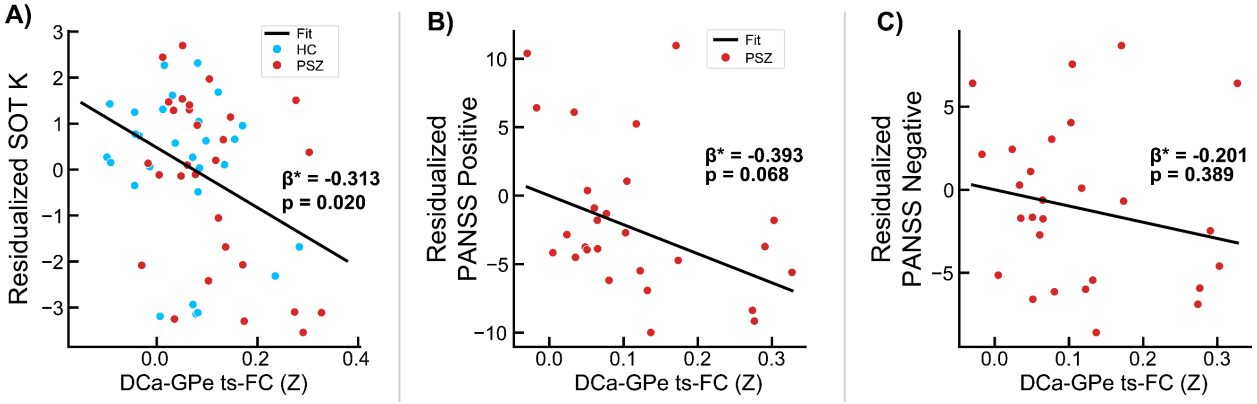

Figure 4. Associations between working memory capacity *K* calculated from self-ordered working memory task (SOT) performance (panel A), Positive and Negative Syndrome Scale (PANSS) positive symptom score (panel B), or PANSS negative symptom score (panel C), and task-state functional connectivity (ts-FC) between dorsal caudate (DCa) and globus pallidus externus (GPe). Associations between *K* and DCa-GPe ts-FC were calculated in all participants (N = 58; blue dots denote healthy controls, while red dots denote people with schizophrenia) controlling for age, sex at birth, and diagnosis, while PANSS symptom associations were calculated in persons with schizophrenia (PSZ; red) only (N = 27; PANSS data were unavailable for two PSZ), controlling for age and sex at birth. Plot inlays show standardized regression coefficient β*.

Table 1. Participant Demographics and Clinical Measures

Participant Characteristic	Task-Based (N = 58)				Resting State (N = 67)			
	PSZ (n = 29)	HC (n = 29)	Effect Size [95% CIs] [a]	P-value	PSZ (n = 37)	HC (n = 30)	Effect Size [95% CIs] [a]	P-value
Functional Magnetic Resonance Imaging Datasets								
Age, Years (SD)	33.4 (12.7)	32.4 (9.7)	-0.02 [-0.28, 0.32]	0.895	32.7 (12.7)	32.5 (9.7)	-0.06 [-0.21, 0.33]	0.659
Sex at Birth, Female (%)	9.0 (31.0%)	9.0 (31.0%)	0.0 [N/A]	1.00	11.0 (29.7%)	8.0 (26.7%)	0.03 [0, 0.29]	0.782
Ethnicity, Hispanic (%)	7.0 (24.1%)	8.0 (27.6%)	0.04 [0, 0.31]	0.764	9.0 (24.3%)	8.0 (26.7%)	0.03 [0, 0.27]	0.827
Race			0.16 [0, 0.41]	0.725			0.10 [0, 0.32]	0.992
African American (%)	14.0 (48.3%)	13.0 (44.8%)			18.0 (48.6%)	13.0 (43.3%)		
Asian (%)	3.0 (10.3%)	3.0 (10.3%)			3.0 (8.1%)	3.0 (10.0%)		
Caucasian (%)	6.0 (20.7%)	8.0 (27.6%)			9.0 (24.3%)	9.0 (30.0%)		
More than one (%)	4.0 (13.8%)	0.0 (0.0%)			3.0 (8.1%)	0.0 (0.0%)		
Other (%)	2.0 (6.9%)	5.0 (17.2%)			4.0 (10.8%)	5.0 (16.7%)		
Handedness[b]			0.19 [0, 0.47]	0.150			0.19 [0, 0.45]	0.111
Ambidextrous (%)	0.0 (0.0%)	0.0 (0.0%)			0.0 (0.0%)	0.0 (0.0%)		
Left (%)	0.0 (0.0%)	2.0 (6.9%)			0.0 (0.0%)	2.0 (6.7%)		
Right (%)	29.0 (100.0%)	27.0 (93.1%)			37.0 (100.0%)	28.0 (93.3%)		
Smoker[c,d] (%)	9.0 (31.0%)	3.0 (10.7%)	-0.26 [-0.53, 0]	0.052	11.0 (30.6%)	3.0 (10.3%)	-0.24 [-0.50,0]	**0.048**
Parental SES[e,f] (SD)	40.3 (13.9)	44.7 (11.2)	0.25 [-0.06, 0.52]	0.102	38.6 (14.3)	44.6 (11.0)	0.33 [-0.05, 0.57]	**0.020**
PANSS Total[g] (SD)	61.6 (18.3)	33.0 (4.8)	-0.92 [-0.98, -0.68]	**1.31×10^{-8}**	65.3 (18.0)	32.4 (2.9)	-2.35 [-3.01, -1.68] [†]	**7.34×10^{-12} [α]**
PANSS General[g] (SD)	31.4 (9.9)	17.0 (2.4)	-0.92 [-0.98, -0.72]	**5.73×10^{-9}**	33.2 (9.8)	16.7 (1.5)	-0.99 [-0.99, -0.96]	**3.25×10^{-11}**
PANSS Negative[g] (SD)	14.4 (4.8)	8.9 (2.7)	-0.72 [-0.87, -0.46]	**6.96×10^{-6}**	15.5 (5.3)	8.6 (2.3)	-0.81 [-0.91, -0.62]	**8.52×10^{-8}**
PANSS Positive[g] (SD)	15.9 (5.4)	7.2 (0.46)	-0.96 [-0.99, -0.78]	**5.87×10^{-10}**	16.6 (5.2)	7.1 (0.27)	-0.97 [-0.99, -0.82]	**4.48×10^{-11}**
CDRS[h] (SD)	3.1 (3.9)	0.17 (0.69)	-0.54 [-0.72, -0.28]	**5.76×10^{-4}**	3.7 (4.2)	0.17 (0.69)	-0.59 [-0.76, -0.35]	**1.81×10^{-4}**
AP Medication-Naïve[k] (%)	14 (48.3%)	—	—	—	19 (51.4%)	—	—	—
Median SOT % Correct (IQR)	88.0 (23.0)	94.0 (8.0)	0.23 [-0.09, 0.50]	0.139	—	—	—	—
Median SOT *k* (IQR)	4.73 (3.42)	5.92 (1.61)	0.23 [-0.08, 0.50]	0.127	—	—	—	—
	Positron Emission Tomography Dataset				***Neuromelanin-Sensitive MRI Dataset***			
	PSZ (n = 7)	HC (n = 4)	Effect Size [95% CIs] [a]	P-value	PSZ (n = 22)	HC (n = 20)	Effect Size [95% CIs] [a]	P-value
Age, Years (SD)	23.1 (6.3)	31.5 (11.9)	0.89 [-0.33, 2.06][†]	0.263[α]	35.1 (13.9)	29.4 (8.5)	-0.18 [-0.50, 0.19]	0.325
Sex at Birth, Female (%)	4 (57.1%)	1 (25.0%)	0.31 [0,0.95]	0.303	8 (36.4%)	7 (35.0%)	0.01 [0,0.27]	0.927
Ethnicity, Hispanic (%)	0 (0.0%)	1 (25.0%)	0.42 [0, 1.05]	0.165	4 (18.2%)	7 (35.0%)	0.19 [0, 0.52]	0.216
Race			0.52 [0, 1.11	0.402			0.28 [0, 0.59]	0.395
African American (%)	3 (42.9%)	2 (50.0%)			12 (54.5%)	8 (40.0%)		
Asian (%)	2 (28.6%)	0 (0.0%)			2 (9.1%)	2 (10.0%)		
Caucasian (%)	2 (28.6%)	1 (25.0%)			4 (18.2%)	6 (30.0%)		
More than one (%)	0 (0.0%)	0 (0.0%)			3 (13.6%)	0 (0.0%)		
Other (%)	0 (0.0%)	1 (25.0%)			1 (4.6%)	4 (20.0%)		
Handedness[b]			0.42 [0, 1.05]	0.165			0.23 [0, 0.56]	0.129
Ambidextrous (%)	0 (0.0%)	0 (0.0%)			0 (0.0%)	0 (0.0%)		
Left (%)	0 (0.0%)	1 (25.0%)			0 (0.0%)	2 (10.0%)		

Right (%)	7 (100.0%)	3 (75.0%)			22 (100.0%)	18 (90.0%)		
Smoker[c] (%)	2 (28.6%)	0 (0.0%)	-0.36 [-0.99, 0]	0.237	6 (27.3%)	3 (15.0%)	-0.15 [-0.48, 0]	0.332
Parental SES[e,f] (SD)	46.8 (15.8)	34.6 (5.9)	-0.43 [-0.85, 0.32]	0.315	42.1 (13.4)	45.7 (10.2)	0.29 [-0.31, 0.89] †	0.336 α
PANSS Total[g] (SD)	78.6 (21.5)	33.5 (4.5)	-2.32 [-3.82, -0.74] †	**0.001α**	64.4 (19.3)	32.8 (3.1)	-2.16 [-2.94, -1.37] †	**2.57 x10^{-7} α**
PANSS General (SD)	39.7 (14.3)	17.8 (2.9)	-1.70 [-3.03, -0.30] †	**0.006α**	32.8 (10.6)	16.6 (1.5)	-0.99 [-1.00, -0.92]	**6.74 x10^{-8}**
PANSS Negative (SD)	19.1 (3.8)	8.8 (1.7)	-2.91 [-4.61, -1.15] †	**1.72 x10^{-4} α**	14.8 (5.1)	9.1 (2.6)	-0.74 [-0.88, -0.45]	**7.64 x10^{-5}**
PANSS Positive (SD)	19.7 (5.6)	7.0 (0)	-2.52 [-4.09, -0.88] †	**0.001α**	16.9 (5.7)	7.1 (0.3)	-2.29 [-3.09, -1.48] †	**1.40 x10^{-7} α**
CDRS[h] (SD)	6.4 (5.3)	0.8 (1.5)	-0.71 [-0.94, -0.03]	0.079	3.4 (4.2)	0.2 (0.8)	-0.55 [-0.75, -0.27]	**0.001**
AP Medication-Naïve[k] (%)	7 (100%)	—	—	—	11 (50.0%)	—	—	—

[a]Effect sizes for continuous variables were calculated with Hedges's g or Cliff's delta *d,* dependent on data normality (determined via Lilliefors test with a null hypothesis that data originates from a normal distribution at significance level p<0.05). Effect sizes for dichotomous and categorical variables were calculated with phi coefficients and Cramér's V, respectively.
[b]Handedness was reported using the Edinburgh Handedness Inventory.
[c]Smoking status defined as current daily nicotine use.
[d]Smoking status was unavailable for 2 participants (1 PSZ and 1 HC) from the resting-state sample and 1 HC from the task-based sample.
[e]Mean Parental SES was reported using the Hollingshead Four Factor Index Scale of Socioeconomic Status scale.
[f]Parental SES data were unavailable for 7 participants (5 PSZ and 2 HC) from the resting-state sample, 4 participants (2 PSZ and 2 HC) from the task-based sample, and 2 HC from the neuromelanin-sensitive MRI sample.
[g]PANSS data were unavailable for 8 participants (4 PSZ and 4 HC) from the resting-state sample, 6 participants (2 PSZ and 4 HC) from the task-based sample, and 3 participants (1 PSZ and 2 HC) from the neuromelanin-sensitive MRI sample.
[h]CDRS data were unavailable for 22 participants (10 PSZ and 12 HC) in the resting-state sample, 16 participants (5 PSZ and 11 HC) in the task-based sample, and 6 participants (2 PSZ and 4 HC) in the neuromelanin-sensitive MRI sample.
[k]All PSZ in this study were antipsychotic-free, defined as no exposure to oral antipsychotic medication for at least 3 weeks, and no exposure to intramuscular antipsychotic medications for at least 6 months, prior to study participation. PSZ were considered to be medication-naïve if they had fewer than 2 weeks of cumulative lifetime exposure to antipsychotic medications, with no prior use of long-acting injectable antipsychotics.
α Indicates use of independent samples t-test, rather than Mann-Whitney U-test, to obtain p-value.
† Indicates effect sizes for continuous variable calculated as Hedges's g, rather than Cliff's delta *d.*
Bold p-values indicate significance at p<0.05 (uncorrected).

Abbreviations: PSZ: People with Schizophrenia; HC: Healthy Controls; SD: standard deviation; SES: socioeconomic status; PANSS: Positive and Negative Syndrome Scale; CDRS: Calgary Depression Scale for Schizophrenia; AP: Antipsychotic; SOT: Self-ordered Working Memory Task; *k*: Working Memory Capacity; IQR: Interquartile Range; CIs: Confidence Intervals.